Cosserat effects in achiral and chiral cubic lattices

Daniel R. Reasa[†], Roderic S. Lakes[*]

May 17, 2022

Department of Engineering Physics, University of Wisconsin, Madison, WI 53706-1687, USA
Keywords (isotropy, chirality, negative Poisson's ratio, auxetic, Cosserat, couple stress)
∗ Corresponding author. email lakes@engr.wisc.edu Phone: +00 608 265 8697
† dreasa@wisc.edu

Preprint: D. Reasa and R. S. Lakes, Cosserat effects in achiral and chiral cubic lattices, Journal of Applied Mechanics (JAM), 86, 111009-1, 6 pages Nov. (2019).

Abstract

Cubic 3D lattices were designed, made by 3D printing, and studied experimentally. One lattice was simple cubic with ribs of diameter 1/5 the cell size. The second lattice was chiral, with spiral ribs. The chiral lattice, but not the achiral lattice, exhibited squeeze-twist coupling with size effects. Squeeze-twist coupling cannot occur in a classically elastic solid but is anticipated by theory in a Cosserat solid. Both lattices exhibited size effects in bending and torsion.

1 Introduction

Truss lattices containing deformable ribs are stiffer than foams of the same density [1]. Because the ribs can carry moments as well as forces, truss lattices can be represented by Cosserat elasticity [2, 3]. Cosserat solids support distributed force (stress) and distributed moments (couple stress).

The constitutive equations for linear isotropic Cosserat [4, 5] (micropolar [6]) elasticity are

$$\sigma_{ij} = 2G\epsilon_{ij} + \lambda\epsilon_{kk}\delta_{ij} + \kappa e_{ijk}(r_k - \phi_k) \tag{1}$$

$$m_{ij} = \alpha\phi_{k,k}\delta_{ij} + \beta\phi_{i,j} + \gamma\phi_{j,i}. \tag{2}$$

The stress σ_{ij} (force per unit area) is in general asymmetric. The resulting moment is balanced by a couple stress m_{ij} (a torque per unit area). Here, κ is an elastic constant, ϕ_k is the rotation of points, called micro-rotation, e_{ijk} is the permutation symbol, and $r_k = \frac{1}{2}e_{klm}u_{m,l}$ is "macro" rotation based on the antisymmetric part of the gradient of displacement u_i. Elastic constants α, β, γ govern the characteristic length scales at which nonclassical effects are to be observed. Also δ_{ij} is the Kronecker delta and ϵ_{ij} is the strain tensor. The quantities λ, G are classical elastic constants. There are six independent Cosserat elastic constants.

These constants may be expressed, as is also done in classical elasticity, as technical elastic constants to enhance physical insight. The constants are Young's modulus E, shear modulus G, Poisson's ratio ν, characteristic length, torsion ℓ_t, characteristic length, bending ℓ_b, coupling number N, polar ratio Ψ. They are expressed:

$$E = \frac{2G(3\lambda + 2G)}{2\lambda + 2G} \tag{3}$$

$$\nu = \frac{\lambda}{2\lambda + 2G} \tag{4}$$

$$\ell_t = \sqrt{\frac{\beta + \gamma}{2G}} \tag{5}$$

$$\ell_b = \sqrt{\frac{\gamma}{4G}} \tag{6}$$

$$N = \sqrt{\frac{\kappa}{2G + \kappa}} \tag{7}$$

$$\Psi = \frac{\beta + \gamma}{\alpha + \beta + \gamma} \tag{8}$$

The characteristic lengths govern the experimental size scale over which one may expect substantial deviations from classical elasticity. For example, size effects occur in the rigidity of rods and bars in torsion [7, 8] and bending [9, 10]. Also, the stress concentration around holes is reduced in comparison with classical predictions [11].

Chiral materials, also called noncentrosymmetric, have an asymmetry in which left and right handedness in the material can be distinguished. Chirality is necessary for optical activity (rotation of the plane of polarization of light as it passes through the material [12]) to occur. Chirality is also necessary for piezoelectric and pyroelectric effects to occur [13]. By contrast, classically elastic materials do not distinguish left from right. The freedom provided in Cosserat elasticity allows for chiral effects in elasticity.

The constitutive equations for a chiral Cosserat solid which is isotropic with respect to direction but not with respect to inversions are [14]:

$$\sigma_{kl} = \lambda\epsilon_{rr}\delta_{kl} + 2G\epsilon_{kl} + \kappa e_{klm}(r_m - \phi_m) + C_1\phi_{r,r}\delta_{kl} + C_2\phi_{k,l} + C_3\phi_{l,k} \tag{9}$$

$$m_{kl} = \alpha\phi_{r,r}\delta_{kl} + \beta\phi_{k,l} + \gamma\phi_{l,k} + C_1\epsilon_{rr}\delta_{kl} + (C_2 + C_3)\epsilon_{kl} + (C_3 - C_2)e_{klm}(r_m - \phi_m). \tag{10}$$

Elastic constants C_1, C_2 and C_3 are associated with the effect of chirality (i.e., noncentrosymmetry). An exact solution for tension / compression of a round chiral Cosserat rod [14] may be used as a guide in seeking new effects including stretch-twist coupling, size effects in tension or compression stiffness, and size effects in Poisson's ratio.

In the absence of chirality, Cosserat effects are known to occur in materials with microstructure. The characteristic length for a 2D square lattice of cell size a is predicted [2] to be $\ell = a/2\sqrt{6}$ within couple stress elasticity which corresponds to Cosserat elasticity with $N = 1$. More recently, Cosserat elastic constants were determined analytically for several lattices [15]. For a 2D square lattice of cell size a, $\ell = a/2\sqrt{6}$ and $N = 1/\sqrt{2}$. Cosserat elastic constants were determined for several 2D lattices containing arrays of circular holes, from experimental tests and finite-element analyses [16]. The values determined for these parameters, particularly the coupling number N, indicate dependence on structure appreciably different from the predictions of lattice theoretical models. The inferred characteristic length was comparable to the size of the holes in the plate. Experimentally, Cosserat effects are known in dense closed cell polymer foams [17, 18] in which isotropy was tested, in low density polymer foams [19], and in negative Poisson's ratio foams. In a truss lattice designed for strong effects [20], size effects in torsion were rigidity were a factor of about 36.

Chiral 2D elastic lattices were conceptualized, made and tested; they also exhibit a Poisson's ratio of -1 [21]. These lattices were shown to behave as Cosserat solids, with a characteristic length

ℓ comparable to the cell size and a large coupling number N [15]. In 2D, stretch twist coupling is not anticipated. Stretch-twist coupling was observed in slender bone specimens [22]; also in fiber bundles in tendon [23]. Squeeze–twist coupling was studied in an elastically isotropic chiral truss lattice [24] containing cubical nodules connected by rib elements.

In the present study, two cubic lattices, one chiral and one achiral, were designed, fabricated via 3D printing, and evaluated experimentally for bending, torsion, and chiral size effects.

2 Methods

Conceptual models of both chiral and achiral lattice materials were constructed in Solidworks and converted to sterolithography (STL) format for printing. The models were printed via Selective Laser Sintering (SLS) out of PA 2200 nylon resin on an EOS P760 machine.

The chiral lattice had spiral ribs with elliptical cross sections measuring 1.5x0.8 mm. The ellipse centers traced a spiral 2 mm in diameter with a pitch of 1.25 mm. The ribs were 5 mm in length, and connected via solid cubes as seen in Figure 1. The achiral lattice had straight circular ribs that were 1.25 mm in diameter and 6.25 mm long for a L/D ratio of 5 as seen in Figure 2. Dimensions were selected to minimize structure size while maintaining printing repeatability.

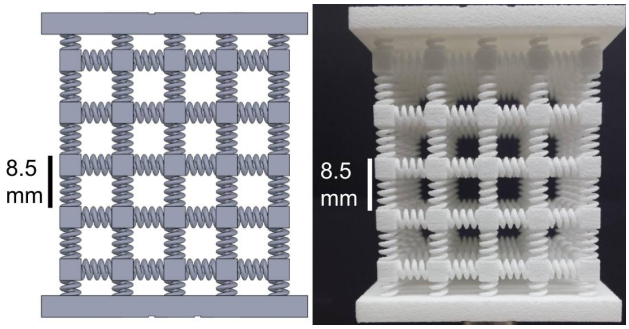

Figure 1: Ideal drawing and 3D printed 4x4x4 cell spiral rib chiral lattice. Scale bar of 8.5mm is the cell size.

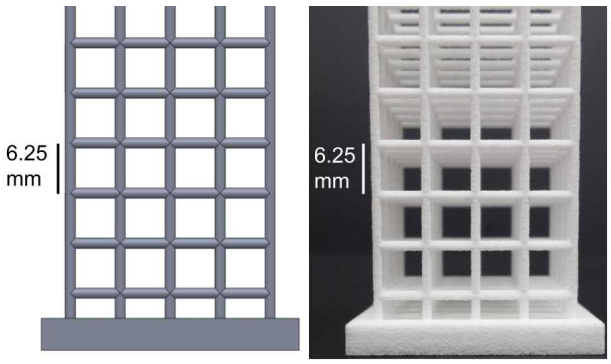

Figure 2: Ideal drawing and 3D printed lower half of the 4x4x12 cell straight rib achiral lattice. Scale bar of 6.25 mm is the cell size

To find the Cosserat characteristic lengths of both the chiral and achiral lattices a broadband

viscoelastic spectrometer (BVS) [20, 25] was used on specimens of varying size at the same aspect ratio. Cubic achiral lattice specimens of 1x1x3, 2x2x6, 3x3x9, 4x4x12, and 5x5x15 cells were tested both in torsion and bending, as were cubic chiral specimens of 1x1x1, 2x2x2, 3x3x3, 4x4x4, and 5x5x5 cells.

The BVS has a pair of Helmholtz coils, one each in bending and torsion, that induce a torque on a magnet attached to the specimens via a ceramic stalk as seen in Figure 3. A mirror on the magnet reflected a laser onto a New Focus 2901 quadrant cell photoreceiver. The receiver was calibrated via a micrometer stage, and the displacement at the receiver was converted into twist angle of the specimen using the calibration value and path length. The magnet was calibrated in the system by attaching it to an aluminum 6061 alloy rod with known properties. The magnet was calibrated once, and all other calibrations were performed both for bending and torsion on every test.

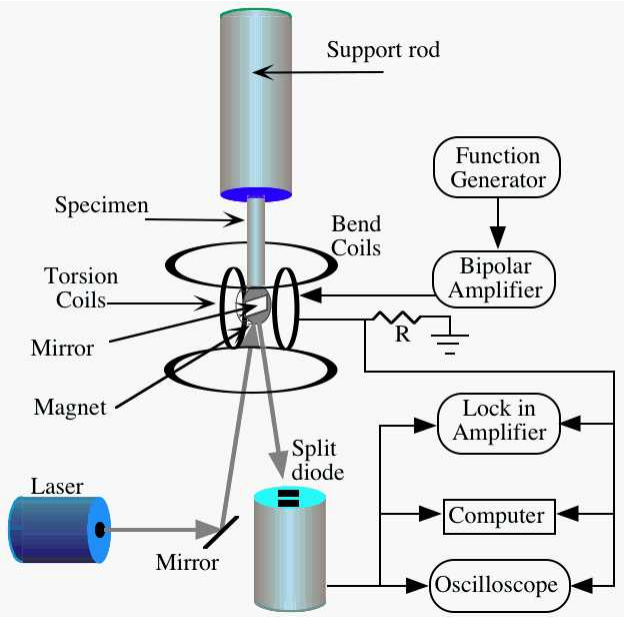

Figure 3: Experimental setup of the Broadband Viscoelastic Spectrometer used to measure size effects in torsion and bending

Tests were performed, following prior methodology [20], by applying a 1 Hz sine wave into the Helmholtz coil, and the resulting receiver voltages were recorded. All tests were conducted at 1 Hz to remove any viscoelastic effects. In the absence of strain gradients Cosserat materials are indistinguishable from classical elastic materials. A screw driven load frame was therefore used to perform pure compression tests to determine the classical Young's modulus E of the material.

To obtain the Cosserat characteristic length in bending, Equation 11 was used [10, 26], where Ω is the ratio of Cosserat rigidity to classical rigidity, ℓ_b is the material's characteristic length in bending, ν is the material's poisson's ratio, β and γ are the Cosserat material constants, a is the sample half width, and N is the material's coupling number. Equation 11 is accurate to $O[(\frac{\ell_b}{2a})^4]$.

$$\Omega = 1 + 24\frac{1+2\nu\beta/\gamma+\nu^2}{1+\nu}(\frac{\ell_b}{2a})^2 - 480(\beta/\gamma+\nu)^2\frac{44-38\nu+3N^2(1-\nu)(13-9\nu)}{N^2(1+\nu)(22-19\nu)}(\frac{\ell_b}{2a})^4 \qquad (11)$$

To obtain the Cosserat characteristic length in torsion, Equation 12 was used [8], where Ω is the ratio of Cosserat rigidity to classical rigidity and $\bar{\ell}_t = \ell_t/a$, $\bar{\ell}_b = \ell_b/a$, $\bar{\alpha} = \alpha/(a^2 G)$, and $\bar{\kappa} = \kappa/G$ are dimensionless forms of the material's Cosserat elastic constants and characteristic lengths in torsion and bending. The material halfwidth is a, and shear modulus is $G = \mu + \kappa/2$. Equation 12 assumes that the coupling number $N = 1$, which was found while fitting the bending data.

$$\Omega = \frac{38}{449} \frac{1796 + 126(449 + 2740\bar{\ell}_t^2 + 3960\bar{\ell}_t^4)\bar{\ell}_t^2 + 693(152 + 2280\bar{\ell}_t^2 + 6615\bar{\ell}_t^4)\bar{\ell}_b^2}{8(19 + 465\bar{\ell}_t^2 + 990\bar{\ell}_t^4) + 1485(6 + 49\bar{\ell}_t^2)\bar{\ell}_b^2} \tag{12}$$

The chiral lattice was investigated for its squeeze twist couple stresses. Five cubic chiral specimens of the same aspect ratio were tested: 1x1x1, 2x2x2, 3x3x3, 4x4x4, and 5x5x5 cells. Testing was done in a dual strain measurement system, seen in Figure 4, utilizing a Linear Variable Differential Transformer (LVDT) for vertical displacement measurements and a laser beam reflected off the specimen onto the same photo-receiver as before for twisting measurements.

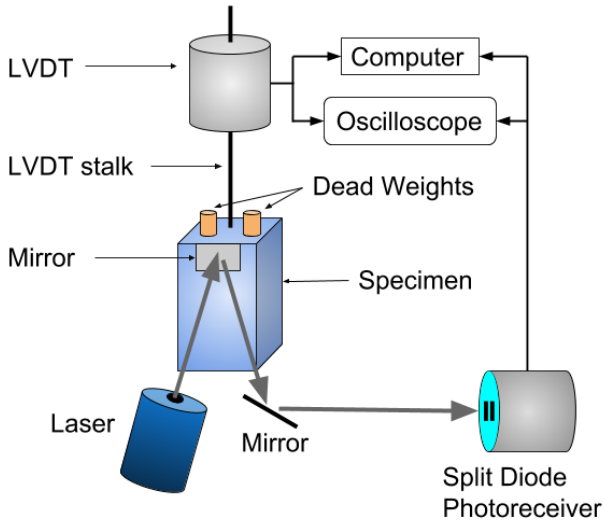

Figure 4: The experimental setup of the dual strain setup used to measure squeeze twist coupling

A vertical stage under the specimen was used to obtain calibration values for the LVDT, and a horizontal stage on the receiver gave calibrations values for the receiver. Dead weights were applied to the the specimen in a symmetric manner to create a uniform stress state. Using the calibration values, specimen dimensions, and path length, the strain coupling was calculated from values measured during repeated application and removal of the weights.

To fit the coupling effects of the material, Equation 13 [14], originally derived for a cylinder of material, was used. Here b_0/ϵ is the coupling value (twist angle per unit length/vertical strain) and the half width of the specimen is R. The characteristic lengths are $\ell_0 = \ell_t = \sqrt{\frac{\beta+\gamma}{2G}}$ $\ell_4 = \ell_t\sqrt{\frac{1-\nu}{\Psi}}$. The K coefficients are dimensionless ratios of elastic constants. $K_0^2 = \frac{(C_1+C_2+C_3)^2}{(\alpha+\beta+\gamma)(\lambda+2G)}$, $K_2 = \frac{\alpha}{(\alpha+\beta+\gamma)}$, $K_3 = \frac{C_1}{(C_1+C_2+C_3)}$, $K_4 = \nu = \frac{\lambda}{\lambda+2G}$

$$\frac{b_0}{\epsilon} = \frac{-K_0 l_4[1 - 2K_3K_4/(1+K_4) + [(K_3+1)K_4/(1+K_4) - K_3)]]/(1-K_4)}{(\frac{R}{2})^2 + l_0^2 + l_4^2[K_0K_3(K_3-1)/(1-K_4^2) + ((1-K_2) - K_0^2(1-K_3^2)/(1+K_4))/2(1-K_4)]} \tag{13}$$

Because available analyses and the present protocol do not suffice to extract all the constants, the equation is simplified as follows before fitting to the measured data.

$$\frac{b_0}{\epsilon} = \frac{l_4 A'}{(\frac{R}{2})^2 + l_0^2 + l_4^2 B'} = \frac{A}{(\frac{R}{2})^2 + B} \tag{14}$$

The theory predicts the ratio of twist to squeeze to be independent of specimen size for small sizes and to roll off in magnitude as $1/R^2$ for large specimen size.

3 Results

Bending size effects in the simple cubic achiral lattice are as shown in Figure 5. The inferred bending characteristic length was $\ell_b = 4.22$ mm, smaller than the cell size of 6.25 mm. The coupling number $N = 1$. The gradient sensitivity ratio was β/γ=0.0001. The goodness of fit was R^2 =0.9807. The asymptote of $E = 26.63$ MPa was measured in pure compression to remove Cosserat effects. The difference in loading rate between the BVS and screw driven frame was neglected due to the small $tan(\delta) = 0.007$ measured in the BVS. A Poisson's ratio of $\nu = 0.0124$ was obtained analytically by multiplying the base material's Poisson's ratio by the area fraction of the cross section.

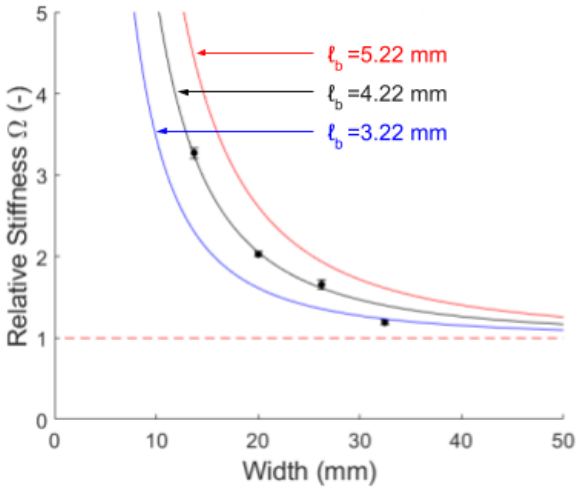

Figure 5: Size effects in bending of the simple cubic achiral lattice. $E = 26.63$ MPa, $\nu = 0.0124$, $\ell_b = 4.22$ mm, $N = 1$, $\beta/\gamma = 0.0001$. The black curve is the best fit to the measured experimental points. Blue and red curves are for $\ell_b = 3.22$ mm and $\ell_b = 5.22$ mm. Dotted red line is for $\ell_b = 0$, a classical response. Error bars are one standard deviation.

Torsion size effects in the simple cubic achiral lattice are as shown in Figure 6. The inferred torsion characteristic length was $\ell_t = 3.13$ mm, considerably smaller than the cell size of 6.25 mm.

The coupling number $N = 1$, and characteristic length in bending $\ell_b = 4.22$ mm, as was determined in bending. The shear modulus $G = 0.66$ MPa was determined while fitting. The goodness of fit was $R^2 = 0.9630$.

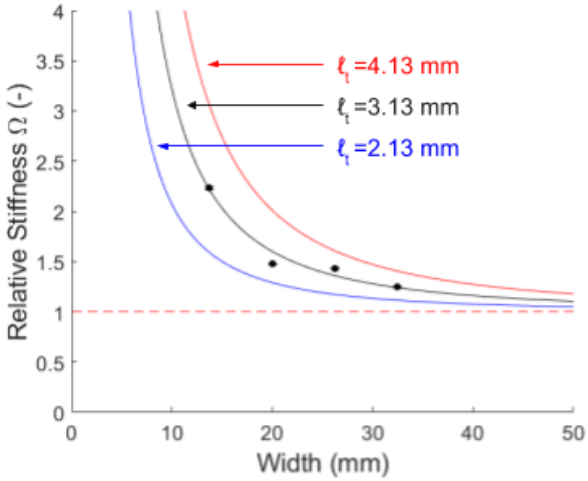

Figure 6: Size effects in torsion of the simple cubic achiral lattice. The black curve is the best fit to the measured experimental points. $G = 0.66$ MPa, $\ell_t = 3.13$ mm, $\ell_b = 4.22$ mm, $N = 1$. Blue and red curves are for $\ell_t = 2.13$ mm and $\ell_t = 4.13$ mm. Dotted red line is for $\ell_t = 0$, a classical response. Error bars are one standard deviation.

A 1x1x3 achiral specimen was tested but was not included in the plotted curve fits as the resulting fit made it clear that the smallest was an outlier of the larger specimens in that the larger specimens were all below the line of best fit. Including the smallest specimen would increase the bending and torsion characteristic lengths by 6% and 15% respectively. The chiral 1x1x1 specimen was included in the plotted fits, as it did not appear to be an outlier. Removing it from analysis would increase the bending and torsion characteristic lengths by 21% and 20% respectively. The analytical assumptions on small ℓ_t/a and ℓ_b/a begin to break down on the smallest specimens, and these specimens only have ribs on the surfaces making a continuum analysis less relevant.

Bending size effects in the chiral cubic lattice are as shown in Figure 7. The inferred bending characteristic length was $\ell_b = 3.83$ mm, smaller than the cell size of 8.5 mm. The coupling number $N = 1$. The gradient sensitivity ratio was β/γ=0.0001. The goodness of fit was $R^2 = 0.9808$. The asymptote of $E = 0.259$ MPa was measured in pure compression to remove Cosserat effects. The difference in loading rate between the BVS and screw driven frame was neglected due to the small $tan(\delta) = 0.009$ measured in the BVS. A Poisson's ratio of $\nu = 0.0668$ was obtained analytically by multiplying the base material's Poisson's ratio by the area fraction of the cross section.

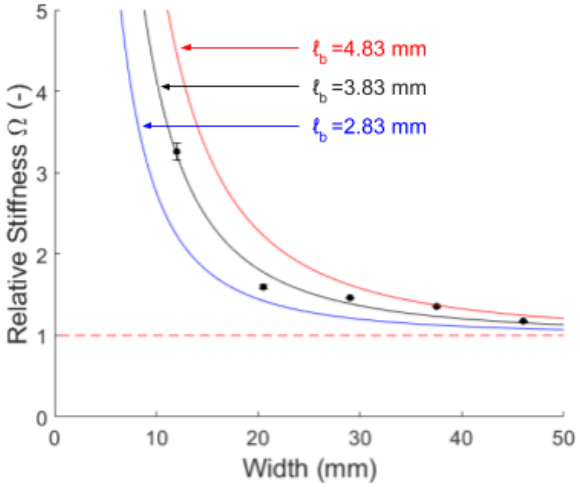

Figure 7: Size effects in bending of the chiral lattice. $E = 0.259$ MPa, $\nu = 0.0668$, $\ell_b = 3.83$ mm, $N = 1$, $\beta/\gamma = 0.0001$. The black curve is the best fit to the measured experimental points. Blue and red curves are for $\ell_b = 2.83$ mm and $\ell_b = 4.83$ mm. Dotted red line is for $\ell_b = 0$, a classical response. Error bars are one standard deviation.

Torsion size effects in the chiral cubic lattice are as shown in Figure 8. The inferred torsion characteristic length was $\ell_t = 6.82$ mm, smaller than the cell size of 8.5 mm. The coupling number $N = 1$, and characteristic length in bending $\ell_b = 3.83$ mm, as was determined in bending. The shear modulus $G = 0.0336$ MPa was determined while fitting. The goodness of fit was $R^2 = 0.9853$.

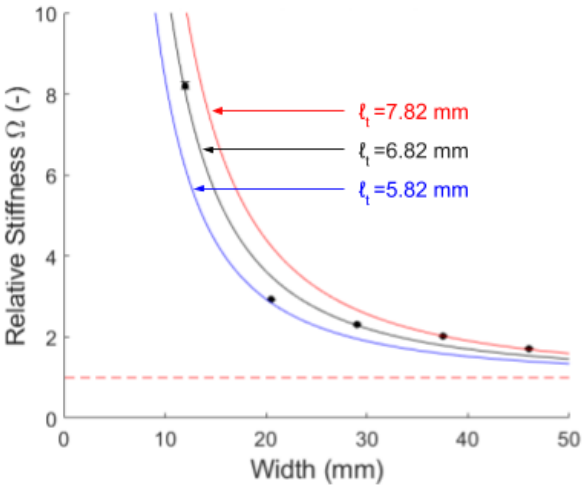

Figure 8: Size effects in torsion of the chiral lattice. The black curve is the best fit to the measured experimental points. $G = 0.0336$ MPa, $\ell_t = 6.82$ mm, $\ell_b = 3.83$ mm, $N = 1$. Blue and red curves are for $\ell_t = 5.82$ mm and $\ell_t = 7.82$ mm. Dotted red line is for $\ell_t = 0$, a classical response. Error bars are one standard deviation.

Squeeze twist coupling between axial strain and torsional twist per length was as shown in Figure

9. The resulting constants in Equation 14 are $A = 0.599$ mm and $B = 8.943\ mm^2$. The goodness of fit was $R^2 = 0.9985$. The resulting fit give a maximum extrapolated coupling of $b_0/\epsilon = 0.067$/mm at 0 radius and $b_0/\epsilon = 0.033$/mm for a single cell. The coupling may be compared with values predicted for a chiral lattice of different design [24] which contained cubical nodules linked by oblique ribs in a chiral configuration. Analysis disclosed twist - squeeze ratio γ/ϵ near 1 over a range of specimen sizes. The twist - squeeze ratio γ/ϵ of strains was measured to be about 1 for a lattice six cells wide [27]. It was not practicable to make such a cubical nodule lattice with a larger number of cells, but the relation $b_0/\epsilon = (\gamma/\epsilon)(1/R)$ enables a comparison to be made. The present lattice has a smaller maximum sensitivity, by a factor of about five, than the cubical nodule based lattice (for the presented single cell specimen $\gamma/\epsilon = 0.2$). Both lattices exhibited a decrease in sensitivity b_0/ϵ with an increase in specimen size.

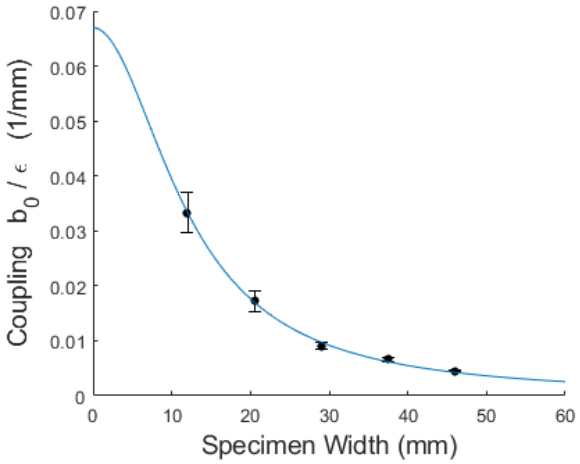

Figure 9: Squeeze twist coupling b_0/ϵ as a function of specimen width. The blue curve is the best fit of Equation 14 to the measured experimental points giving $A = 0.599$ mm and $B = 8.943\ mm^2$. Error bars are one standard deviation.

The achiral lattice with straight ribs was tested in the squeeze twist setup, and found to have a coupling of $b_0/\epsilon = -0.001$ and standard deviation of 530%. The standard deviations on the chiral lattices were between 3% and 12%. Therefore the squeeze twist coupling of the achiral lattice is zero within the resolution of the experiment, so the structurally achiral lattice is elastically achiral as well.

All of the analysis assumed that the specimens were elastically isotropic in nature, while in reality they likely would be elastically cubic corresponding to their structure. This has an effect on the calculated material characteristic lengths, however no analytical solutions for elastically cubic Cosserat materials exist. Consequences of the cubic anisotropy include relaxation of the usual isotropic relation among Young's modulus, shear modulus and Poisson's ratio; also the interrelation among isotropic Cosserat constants as found in isotropic foams [18] does not apply to cubic materials. Additionally, the squeeze twist analytical solution assumed a circular cross section, while the tested specimens were square in cross section. The bending and torsion analysis assumed the specimen was achiral. Again, no proper alternative theory currently exists.

To summarize, Cosserat effects were observed in cubic lattices. For the achiral lattice with straight ribs, size effects in torsion and bending revealed characteristic lengths about half the cell size. No coupling between compression and torsion (squeeze twist coupling) was observed. By

contrast, lattices designed with complex rib shapes to enhance Cosserat effects [20] exhibited larger characteristic lengths comparable to the cell size and larger size effects, up to a factor of 36. Cells or ribs with complex shapes do not guarantee large Cosserat effects. A negative Poisson ratio lattice was found to have characteristic lengths about one third the cell size [28]. Open cell foams of low density have characteristic lengths larger than the cell size [19]. The measured characteristic lengths of the straight rib lattice were nonetheless larger than those predicted by a two dimensional homogenization theory [15]. The distinction between 2D and 3D is likely to be crucial in this comparison.

The straight rib achiral lattice, though not designed to exhibit nonclassical effects, nevertheless exhibited Cosserat type size effects. One may reasonably expect that other truss lattices that have been recently developed will also exhibit nonclassical effects.

The chiral lattice exhibited size effects in torsion and in bending. The Cosserat characteristic length in torsion was less than half the cell size. Squeeze twist coupling was observed in compression of the chiral lattice. This effect decreased with specimen size as anticipated by theory [14]. The squeeze twist sensitivity for small specimens was about one fifth that of a chiral lattice with cubical nodules and oblique connecting ribs [27].

4 Conclusion

The chiral lattice exhibited squeeze-twist coupling and the achiral lattice did not. Size effects were observed in the squeeze-twist coupling as anticipated by analysis. Size effects were also observed in bending and torsion of all samples as anticipated. However, the relations between the measured Cosserat constants were relaxed by material anisotropy.

References

[1] Deshpande, V., Fleck, N., and Ashby, M.F., Effective properties of the octet truss lattice material. J. Mech. Phys. Solids **49**, 1747-1769 (2001)

[2] Banks C.B., Sokolowski M., On certain two-dimensional applications of the couple-stress theory. Int. J. Solids Struct. **4**, 15-29 (1968)

[3] Askar A, Cakmak A.S., A structural model of a micropolar continuum. Int. J. Engng. Sci. **6**(10), 583-589 (1968)

[4] Cosserat, E., and Cosserat, F., *Theorie des Corps Deformables*. Hermann et Fils, Paris (1909)

[5] Mindlin, R.D., Stress functions for a Cosserat continuum. Int. J. Solids Struct. **1**(3), 265-271 (1965)

[6] Eringen, A.C., Theory of micropolar elasticity. In Fracture Vol. **1**, 621-729 (edited by H. Liebowitz), Academic Press, New York (1968)

[7] Gauthier, R.D., and Jahsman, W.E., A Quest for Micropolar Elastic Constants. J. of Appl. Mech. **42**(2), 369-374 (1975)

[8] Drugan W.J., and Lakes, R.S., Torsion of a Cosserat elastic bar with square cross section: theory and experiment. Z. Angew. Math. Phys. **69**(2) (2018). https://doi.org/10.1007/s00033-018-0913-1

[9] Krishna Reddy, G.V., and Venkatasubramanian, N.K., On the Flexural Rigidity of a Micropolar Elastic Circular Cylinder. J. of Appl. Mech. **45**(2), 429-431 (1978)

[10] Lakes, R.S., and Drugan, W.J., Bending of a Cosserat Elastic Bar of Square Cross Section: Theory and Experiment. J. of Appl. Mech. **82**(9) (2015). https://doi.org/10.1115/1.4030626

[11] Mindlin, R.D., Influence of couple-stresses on stress concentrations. Exp. Mech. **3**(1), 1-7 (1963)

[12] Bose, J.C., On the rotation of plane of polarisation of electric waves by a twisted structure. Proc. R. Soc. Lond. **63**, 146-152 (1898)

[13] Nye, J.F., *Physical Properties of Crystals*. Oxford University Press, Clarendon (1976)

[14] Lakes, R.S., and Benedict, R.L., Noncentrosymmetry in micropolar elasticity. Int. J. of Engng. Sci. **20**(10), 1161-1167 (1982)

[15] Spadoni A., and Ruzzene M., Elasto-static micropolar behaviour of a chiral auxetic lattice. J. Mech. Phys. Solids **60**, 156-171 (2012)

[16] McGregor M., and Wheel M.A., On the coupling number and characteristic length of micropolar media of differing topology. Proc. R. Soc. A **470**: 20140150 (2014). http://dx.doi.org/10.1098/rspa.2014.0150

[17] Lakes, R.S., Experimental Microelasticity of Two Porous Solids. Int. J. Solids Struct. **22**, 55-63 (1986)

[18] Rueger, Z., and Lakes, R.S., Experimental study of elastic constants of a dense foam with weak Cosserat coupling. J. of Elasticity, (2018). https://doi.org/10.1007/s10659-018-09714-8

[19] Rueger, Z., and Lakes, R.S., Experimental Cosserat elasticity in open cell polymer foam. Philos. Mag. **96**(2), 93-111 (2016)

[20] Rueger, Z., and Lakes, R.S., Strong Cosserat elasticity in a transversely isotropic polymer lattice. Phys. Rev. Lett. **120**, 065501 (2018). https://doi.org/10.1103/PhysRevLett.120.065501

[21] Prall, D., and Lakes, R.S., Properties of a chiral honeycomb with a Poisson's ratio of -1. Int. J. of Mech. Sci. **39**(3), 305-314 (1997)

[22] Lakes, R.S., Is bone elastically noncentrosymmetric? Proc. 34th ACEMB. Houston (1981)

[23] Buchanan, K., Lakes, R.S., and Vanderby, R., Chiral behavior in rat tail tendon fascicles. J. of Biomech. **64**, 206-211 (2017)

[24] Ha, C.S., Plesha, M.E., and Lakes, R.S., Chiral three-dimensional isotropic lattices with negative Poisson's ratio. Phys. Status Solidi B **253**(7), 1243-1251 (2016)

[25] Lee, T., Lakes, R.S., and Lal, A., Resonant ultrasound spectroscopy for measurement of mechanical damping: Compasison with broadband viscoelastic spectroscopy. Rev Sci. Instrum. **71**, 2855 (2000). https://doi.org/10.1063/1.1150703

[26] Drugan, W.J., private communication.

[27] Li, J., Ha, C.S., and Lakes, R.S., Observation of squeeze twist coupling in a chiral three-dimensional isotropic lattice (in preparation)

[28] Rueger, Z., Li, D., Lakes, R. S., Observation of Cosserat elastic effects in a tetragonal negative Poisson's ratio lattice, Physica Status Solidi B, **254**, 1600840, 6 pages, (2017)